

# Grappa - A Machine Learned Molecular Mechanics Force Field

Leif Seute<sup>1</sup> Eric Hartmann<sup>1,2</sup> Jan Stühmer<sup>1,3</sup> Frauke Gräter<sup>1,2</sup>

## Abstract

Simulating large molecular systems over long timescales requires force fields that are both accurate and efficient. In recent years, E(3) equivariant neural networks have lifted the tension between computational efficiency and accuracy of force fields, but they are still several orders of magnitude more expensive than classical molecular mechanics (MM) force fields. Here, we propose a novel machine learning architecture to predict MM parameters from the molecular graph, employing a graph attentional neural network and a transformer with symmetry-preserving positional encoding. The resulting force field, Grappa, outperforms established and other machine-learned MM force fields in terms of accuracy at the same computational efficiency and can be used in existing Molecular Dynamics (MD) engines like GROMACS and OpenMM. It predicts energies and forces of small molecules, peptides, RNA and — showcasing its extensibility to uncharted regions of chemical space — radicals at state-of-the-art MM accuracy. We demonstrate Grappa’s transferability to macromolecules in MD simulations, during which large protein are kept stable and small proteins can fold. Our force field sets the stage for biomolecular simulations close to chemical accuracy, but with the same computational cost as established protein force fields.

## 1. Introduction

Machine learned force fields are currently reshaping the field of computational chemistry and Molecular Dynamics (MD) simulations. E(3)-equivariant neural networks [1–5] are capable of predicting energies and forces of small molecules to great accuracy with lower computational cost than quantum mechanical (QM) methods. However, these models are

several orders of magnitude more expensive than Molecular Mechanics (MM) force fields, which employ a simple physics-inspired functional form to parametrize the potential energy surface of a molecular system, hence trading off accuracy in favor of efficiency. For MD simulations of large systems such as proteins and nucleic acids, MM force fields are well established and widely used. Traditional MM force fields rely on lookup tables with a finite set of atom categories that describe local chemical environments for parameterization. Recently, the Espaloma approach [6] has demonstrated that machine learning can be used to increase the accuracy of MM force fields by learning to assign parameters based on a graph representation of the molecule with hand-crafted chemical features such as orbital hybridization states.

In this work, we propose a novel machine learning architecture, Grappa (Graph Attentional Protein Parametrization), to learn MM parameters directly from the molecular graph, improving accuracy on a broad range of chemical space and eliminating the need for hand-crafted features. Grappa employs a graph attentional neural network to predict local chemical environments followed by a transformer [7] with symmetry-preserving positional encoding. Since MM parameters only have to be predicted once per molecule, Grappa can be incorporated into highly optimized MM engines such as GROMACS [8] and OpenMM [9]. This allows energy and force evaluations with the same computational cost as traditional force fields, at state-of-the-art MM accuracy.

We show that Grappa outperforms traditional MM force fields and Espaloma on the Espaloma dataset [10], which contains over 14,000 molecules and more than 1 million states, covering small molecules, peptides and RNA. Since Grappa uses no hand-crafted chemical features, it can be extended to uncharted regions of chemical space, which we demonstrate on the example of peptide radicals. Grappa is transferable to macromolecules such as proteins, which it keeps stable during MD over nanosecond timescales. Starting from an unfolded initial state, MD simulations of small proteins parametrized by Grappa recover experimentally determined folding structures of small proteins, suggesting that Grappa captures the physics underlying protein folding.

<sup>1</sup>Heidelberg Institute for Theoretical Studies, Schloss-Wolfsbrunnengasse 35, 69118 Heidelberg, Germany  
<sup>2</sup>Interdisciplinary Center for Scientific Computing, Heidelberg University, INF 205, 69120 Heidelberg, Germany  
<sup>3</sup>Institute for Anthropomatics and Robotics, Karlsruhe Institute of Technology, Kaiserstr. 12, 76131 Karlsruhe, Germany. Correspondence to: Leif Seute <leif.seute@h-its.org>.

### 1.1. Molecular Mechanics

Given a molecular graph, MM expresses the potential energy of a system as a sum of contributions from different interactions. Bonded interactions are described by functions of E(3)-invariant internal coordinates such as the lengths  $r_{ij}$  of bonds between two atoms, angles  $\theta_{ijk}$  between three consecutive atoms and dihedrals  $\phi_{ijkl}$  of two planes spanned by four atoms. For the dihedrals, one considers interactions between four atoms that are either consecutively bonded (torsions) or where three atoms are bonded to a central atom (impropers), which do not reflect an independent degree of freedom but are used to maintain planarity of certain chemical groups. One commonly uses harmonic potentials for bond stretching and angle bending and a periodic function for the dihedral potential. The potential energy of all interactions along bonds then is given by

$$\begin{aligned}
 E_{\text{bonded}}(\mathbf{x}) = & \sum_{(ij) \in \text{bonds}} k_{ij} (r_{ij} - r_{ij}^{(0)})^2 \\
 & + \sum_{(ijk) \in \text{angles}} k_{ijk} (\theta_{ijk} - \theta_{ijk}^{(0)})^2 \\
 & + \sum_{(ijkl) \in \text{dihedrals}} \sum_{n=1}^{n_{\text{periodicity}}} k_{ijkl} \cos(n\phi_{ijkl}), \quad (1)
 \end{aligned}$$

with the equilibrium values (of bonds and angles)  $r_{ij}^{(0)}$  and  $\theta_{ijk}^{(0)}$ , and the force constants  $k_{ij}$ ,  $k_{ijk}$  and  $k_{ijkl}$ , as the set of MM parameters, which we denote as

$$\xi \equiv \{ \xi_{ij\dots}^{(l)} \mid l \in \{ \text{bonds, angles, torsions, impropers} \} \}. \quad (2)$$

For the dihedral potential in Grappa, we choose a Fourier series with the constraint that the dihedral potential is extremal at and symmetric around zero, which eliminates the need for sine terms. Additionally, atom pairs that are not included in such N-body bonded interaction terms contribute to the potential energy through pairwise nonbonded interaction, typically described by Lennard-Jones and Coulomb potentials.

Traditional MM force fields define a finite set of atom types determined by hand-crafted rules, which are used to assign the free parameters  $\{k_{ij}, r_{ij}^{(0)}, \dots\}$  based on lookup tables for possible combinations of atom types. In Grappa, we replace this scheme by learning the parameters from the molecular graph directly, which allows for a more flexible and transferable description of the potential energy surface.

A fundamental limitation of standard MM is the assumption of a constant molecular graph topology, which is enforced by the use of harmonic bond potentials. While this restricts accuracy and prohibits the description of bond-changing chemical reactions, the physical interpretability of the potential energy function ensures that simulated systems remain

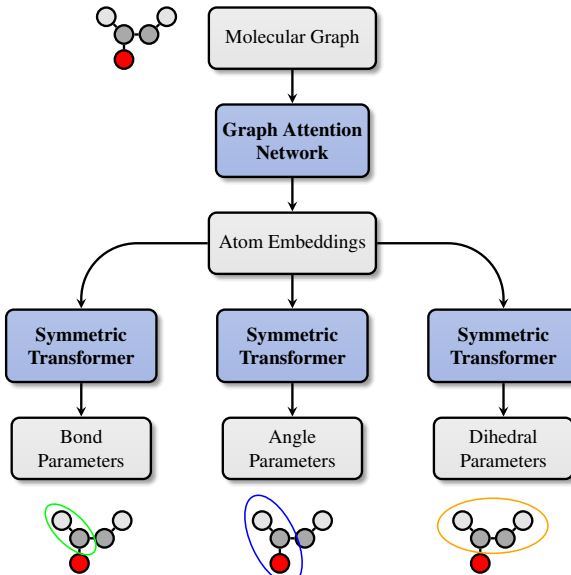


Figure 1: Grappa predicts MM parameters in two steps. First, atom embeddings are predicted from the molecular graph with a graph neural network. Then, transformers with symmetric positional encoding followed by permutation invariant pooling maps the embeddings to MM parameters with desired permutation symmetries. Once the MM parameters are predicted, the potential energy surface can be evaluated with MM-efficiency for different spatial conformations.

stable, even in states that are poorly described by the force field.

## 2. Grappa

Inspired by the atom typing with hand-crafted rules in traditional MM force fields and in analogy to [6], Grappa first predicts  $d$ -dimensional atom embeddings,

$$\nu = \{ \nu_i \in \mathbb{R}^d \mid i \in \mathcal{V} \}, \quad (3)$$

which can represent local chemical environments that are encoded in the structure of the molecular graph  $\mathcal{G} = (\mathcal{V}, \mathcal{E})$ , where the set of nodes  $\mathcal{V}$  represents the atoms and the set of edges  $\mathcal{E}$  represents the bonds. In a second step (Figure 1), for each interaction type  $l$  MM parameters  $\xi^{(l)}$  are predicted from the embeddings of the atoms involved in the respective energy contribution,

$$\xi_{ij\dots}^{(l)} = \psi^{(l)}(\nu_i, \nu_j, \dots), \quad (4)$$

using a transformer  $\psi^{(l)}$  that is invariant under certain permutations. With the energy function of MM, the predicted parameter set  $\xi$  defines a potential energy surface, which can finally be evaluated for different spatial conformations

$\mathbf{x}$  of the molecule,

$$E(\mathbf{x}) = E_{\text{MM}}(\mathbf{x}, \xi). \quad (5)$$

Since the mapping from molecular graph to energy is differentiable with respect to the model parameters and spatial positions, it can be optimized on predicting QM energies and forces end-to-end. Notably, the machine learning model does not depend on the spatial conformation of the molecule, thus it has to be evaluated only once per molecule and the computational cost of each subsequent energy evaluation is given by the MM energy function.

Grappa currently only predicts bonded MM parameters since the highly nonlinear energy function for nonbonded interactions impedes optimization. The nonbonded parameters are taken from established MM force fields that can reproduce solute interactions and melting points, which we expect to be strongly dependent on nonbonded interactions.

### 2.1. Permutation symmetries in MM

For the mapping from atom embeddings  $\nu$  to MM parameters, we postulate certain permutation symmetries that our model should respect. To derive these symmetries, we consider the energy function of MM as a decomposition into contributions from subgraphs of the featurized molecular graph that correspond to bonds, angles, torsions and improper dihedrals. We demand invariance of the energy contribution under node permutations that induce isomorphisms of the respective subgraph. For bonds, angles and torsions, these permutations leave the respective spatial coordinate invariant, thus we can simply achieve invariance of the energy contribution by demanding invariance of the MM parameters,

$$\xi_{ij}^{(\text{bond})} = \xi_{ji}^{(\text{bond})}, \quad (6)$$

$$\xi_{ijk}^{(\text{angle})} = \xi_{kji}^{(\text{angle})}, \quad (7)$$

$$\xi_{ijkl}^{(\text{torsion})} = \xi_{lkji}^{(\text{torsion})}. \quad (8)$$

For improper dihedrals, however, not all subgraph isomorphisms leave the dihedral angle invariant and demanding parameter invariance under those permutations would lead to an energy contribution that is not invariant. In Grappa, we solve this problem by decomposing the improper torsion contributions into three terms, as described in A.4.

### 2.2. The Grappa architecture

To predict atom embeddings from the molecular graph, Grappa employs a graph attentional neural network inspired by the transformer architecture [7]. Multi-head dot-product attention on graph edges [11] is followed by nodewise feed-forward layers. We use residual connections [12] and layer normalization [13], which has been demonstrated to enhance the expressivity of the attention layer [14].

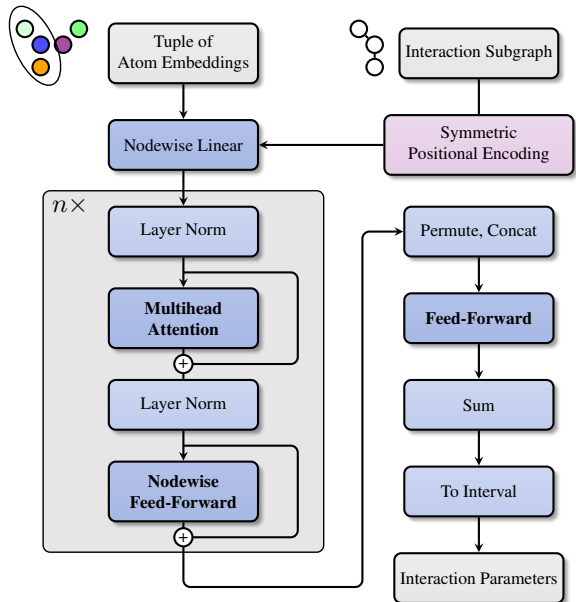


Figure 2: Architecture of the symmetric transformer: Atom embeddings are equipped with a permutation invariant positional encoding determined by the subgraph they represent. They are then passed through  $n = 3$  permutation equivariant transformer layers, symmetry-pooled and mapped to the possible range of the respective parameter.

For the map from these embeddings to MM parameters, it is desirable to use an architecture that respects the permutation symmetries (Eqs. 6 - 8) by design, constraining the space of possible models to those that are physically sensible. In the spirit of equivariant machine learning, we use permutation equivariant layers followed by final symmetric pooling. However, since we do not require invariance under all permutations but only under permutations as defined in Eqs. 6 - 8, we can increase expressivity by allowing the model to break symmetries that are not required.

Following these considerations, we use a transformer architecture based on multi-head dot-attention with a positional encoding that is invariant under the required symmetries but can break others. For example for angles, this positional encoding is given by

$$(\nu_i, \nu_j, \nu_k) \mapsto (\nu_i \oplus 0, \nu_j \oplus 1, \nu_k \oplus 0), \quad (9)$$

where the  $\oplus$  operation appends the respective value to the node feature vector, making it invariant under  $ijk \rightarrow kji$  but not under e.g.  $ijk \rightarrow jik$ . After these equivariant layers, we apply a multilayer perceptron (MLP) on the concatenated permuted node embeddings and sum over the desired set of permutations  $\mathcal{P}$ ,

$$z_{ij\dots} = \sum_{\sigma \in \mathcal{P}} \text{MLP}([\nu_{\sigma(i)}, \nu_{\sigma(j)}, \dots]), \quad (10)$$

defining a symmetry pooling operation with  $\mathcal{P}$ -invariant output. We call this combination of permutation invariant positional encoding with permutation equivariant layers and symmetric pooling the *symmetric transformer*, which is illustrated in Figure 2. The symmetric transformer can be generalized to permutation symmetries of arbitrary sub-graphs by using the eigenvectors of the graph Laplacian [15] as positional encoding.

Finally, we map to the range of physically sensible parameters, e.g.  $(0, \infty)$  for bond and angle force constants or  $(0, \pi)$  for equilibrium angles  $\theta^{(0)}$ . To this end, we use scaled and shifted versions of ELU and the sigmoid function as described in A.2.3. While one could also use the exponential for mapping to  $(0, \infty)$ , ELU’s linear behaviour towards large inputs is favorable for producing stable gradients during optimization. With the scaling we ensure that a normally distributed output of the neural network is mapped to a distribution with mean and standard deviation that is suitable for the respective MM parameter, which can be seen as a normalization technique [13]. For predicting dihedral parameters  $\xi_{ijkl}$ , we use a sigmoid gate, which allows the model to suppress dihedral modes that are not needed.

As input feature, we use one-hot encodings of the atomic number, the number of neighbors of the respective node and membership in loops of length 3 to 8, which can be directly calculated from the molecular graph. The assignment of nonbonded MM parameters is done using a traditional force field of choice. Since the optimal bonded parameters predicted by Grappa may depend on the scheme by which nonbonded parameters are assigned, we pass a sinusoidal encoding [7] of the partial charge of each atom as input feature to Grappa, which also allows to encode the total charge of a molecule without breaking graph symmetries as one would potentially do by using the formal charge instead. For the extension to proteins in section 3.3, we train Grappa to be compatible with two different schemes of nonbonded parameter assignment, which we encode as additional input feature. These schemes are a) what we call the AM1-BCC scheme, with Lennard-Jones parameters from the OpenFF-2.0.0 force field and partial charges from the semi-empirical method AM1-BCC [16] and b) what we call the ff99SB scheme, with Lennard-Jones parameters and partial charges from the established Amber ff99SB-ILDN [17] protein force field.

### 2.3. Training

We train Grappa to minimize the mean squared error (MSE) between QM energies  $E_{\text{QM}}$  and forces  $-\nabla_{\mathbf{x}}E_{\text{QM}}$ , whose contribution we weight by the hyperparameter  $\lambda_F$ , and its prediction,  $E$  and  $\nabla_{\mathbf{x}}E$  respectively, which includes the non-learnable nonbonded contribution. At the start of training, we also include the deviation of predicted bond, angle

and torsion MM parameters to those of a given traditional force field, weighted by  $\lambda_{\text{trad}}$  and, for regularization, the  $L_2$  norm of dihedral MM parameters  $\xi_{ijkl}^{(\text{dih})}$ , weighted by  $\lambda_{\text{dih}}$  as in [10]. That is, we use the loss function

$$\mathcal{L} = \text{MSE}(E, E_{\text{QM}}) + \lambda_F \text{MSE}(\nabla_{\mathbf{x}}E, \nabla_{\mathbf{x}}E_{\text{QM}}) + \lambda_{\text{MM}} \text{MSE}(\xi, \xi_{\text{trad}}) + \lambda_{\text{dih}} \|\xi^{(\text{dih})}\|_2^2. \quad (11)$$

Since MM can only predict energy differences of states, not formation energies, we subtract the mean of target and predicted energies for each molecule. As shown previously for other machine learned force fields [18, 5], we find training on forces  $-\nabla_{\mathbf{r}}E$  in addition to energies important also in our setting, for two reasons. First, the energy is a global, pooled quantity and thus less expressive than the forces, which are local and by a factor of  $3N$  more numerous. Second, as shown in [19], learning derivatives of the target with respect to the input can lead to improved generalization and data efficiency, effectively smoothing the learned potential energy surface.

The motivation for the different terms in the loss function, details on the training procedure and hyperparameters for all models mentioned in Sections 3 and 4 can be found in A.3.

## 3. Results

### 3.1. Benchmark results

To demonstrate that Grappa is the current state of the art MM force field, we train and evaluate a Grappa model on the dataset reported in the follow-up paper [10] to Espaloma, which contains 17,427 unique molecules and over one million conformations. Our training and test partition is identical with the one from Espaloma, where the molecules were divided into 80% training, 10% validation and 10% test set, based on isomeric SMILES strings. The dataset covers small molecules, peptides and RNA with states sampled from the Boltzmann distribution at 300 K and 500 K, from optimization trajectories and from torsion scans. The non-bonded contribution is calculated using the OpenFF-2.0.0 force field [20] and partial charges from the AM1-BCC method, as in Espaloma.

For all types of molecules, Grappa outperforms established MM force fields and Espaloma in terms of energy and force accuracy on Boltzmann-sampled states as shown in Table 1 and Figure 3a. While the Boltzmann samples are the more relevant benchmarking data for using Grappa in MD simulations, we also compared performance on torsion scans and optimization trajectories (Table A4). There, we find Grappa and Espaloma to be competitive, while Grappa is more accurate for forces and less accurate for energies. This is also the case if Grappa is only trained on a fraction of Espaloma’s training set (Figure A9), indicating high data efficiency.

Grappa - A Machine Learned Molecular Mechanics Force Field

Dataset	Test Mols	Confs		Grappa	Espaloma	Gaff-2.11	ff14SB, RNA.OL3	Mean Predictor
SPICE-Pubchem	1411	60853	<i>Energy</i>	<b>2.3</b>	<b>2.3</b>	4.6		18.4
			<i>Force</i>	<b>6.1</b>	6.8	14.6		23.4
SPICE-DES-Monomers	39	2032	<i>Energy</i>	<b>1.3</b>	1.4	2.5		8.2
			<i>Force</i>	<b>5.2</b>	5.9	11.1		21.3
SPICE-Dipeptide	67	2592	<i>Energy</i>	<b>2.3</b>	3.1	4.5	4.6	18.7
			<i>Force</i>	<b>5.4</b>	7.8	12.9	12.1	21.6
RNA-Diverse	6	357	<i>Energy</i>	<b>3.3</b>	4.2	6.5	6.0	5.4
			<i>Force</i>	<b>3.7</b>	4.4	16.7	19.4	17.1
RNA-Trinucleotide	64	35811	<i>Energy</i>	<b>3.5</b>	3.8	5.9	6.1	5.3
			<i>Force</i>	<b>3.6</b>	4.3	17.1	19.7	17.7

Table 1: Accuracy of Grappa, Espaloma 0.3 [10] and established MM force fields on test molecules of the Espaloma dataset. We only display the states that are sampled from the Boltzmann distribution, optimization trajectories, torsion scans and uncertainties are shown in Table A4. We report the RMSE of molwise-centered energies in kcal/mol and the componentwise RMSE of forces in kcal/mol/Å. Gaff-2.11 [21] is a general-purpose force field, ff14SB [22] is an established protein force field and RNA.OL3 [23] is specialized to RNA. The datasets SPICE-Pubchem and SPICE-DES-Monomers are subsets of the SPICE dataset [24] and contain small molecules, the other datasets contain peptides and RNA. As in Espaloma, we bootstrap the set of test molecules 1000 times and report the mean of the RMSEs; their standard deviation is given in Table A4.

### 3.2. Latent space

To generalize across the broad range of chemical space covered by the training set, our model has to learn highly informative atom embeddings that capture the local environment in the molecular graph. For interpreting this latent representation, we apply a two-dimensional principal component analysis on a set of predicted atom embeddings (3) of test molecules (Figure 3b). It turns out that the two principal components can be related to the periodic table of elements, which is thus learned implicitly by Grappa.

### 3.3. Extension to proteins

Especially for large biomolecules, force fields are not only required to predict energies and forces as accurately as possible, but their predictions should behave in such a way that certain macroscopic properties such as stability and consistency with experimentally determined folding states are fulfilled in MD simulations. Grappa is well suited to overcome the gap between empirically validated, established protein force fields and machine learned force fields.

We show that Grappa can be trained to predict bonded parameters that are consistent with nonbonded parameters from both the established Amber ff99SB-ILDN force field [17] and from the AM1-BCC method. This enables accurate prediction of energies and forces while using established nonbonded parameters, which we expect to be primarily responsible for properties like stability and folding states. Since Grappa does not rely on hand-crafted chemical input features, its incorporation into established MD engines for biomolecules, like GROMACS [8], is straight-

forward and its workflow can be scaled to large molecules; only connectivity and atomic numbers are required as additional input features. By the hyperparameter  $\lambda_{\text{trad}}$  and its MM formulation, it also offers the option to smoothly and consistently interpolate between established force fields and entirely machine learned force fields.

To make Grappa applicable to proteins, we train it on the Grappa-1.1 dataset, which is an extension of the Espaloma dataset by dipeptides containing the non-standard residues hydroxyproline and DOPA (dihydroxyphenylalanine), uncapped peptides and, demonstrating Grappa’s capability to parametrize rather uncommon molecules, peptide radicals, all with nonbonded parameters from Amber ff99SB-ILDN. This choice is motivated by future applications of Grappa to collagen and radicals therein, but here serves as a demonstration of the ease of extending Grappa to chemistries outside of standard biomolecular force fields. To create these additional datasets, we calculate DFT energies and gradients of states that were sampled from MD simulations performed with traditional force fields at 300K, where we increase the temperature to 500 K in between the samplings to enrich conformational diversity, as described in A.5.

In Table 2, we report Grappa’s accuracy on a subset of the Grappa-1.1 dataset. We find that our model, after being trained with nonbonded parameters from the ff99SB scheme or the AM1-BCC scheme, can predict energies and forces of dipeptides with both schemes to similar accuracy. On the other datasets from Espaloma, Grappa remains competitive if trained on both charge methods and the broader range of molecules, as can be seen in Table A5. For the radical

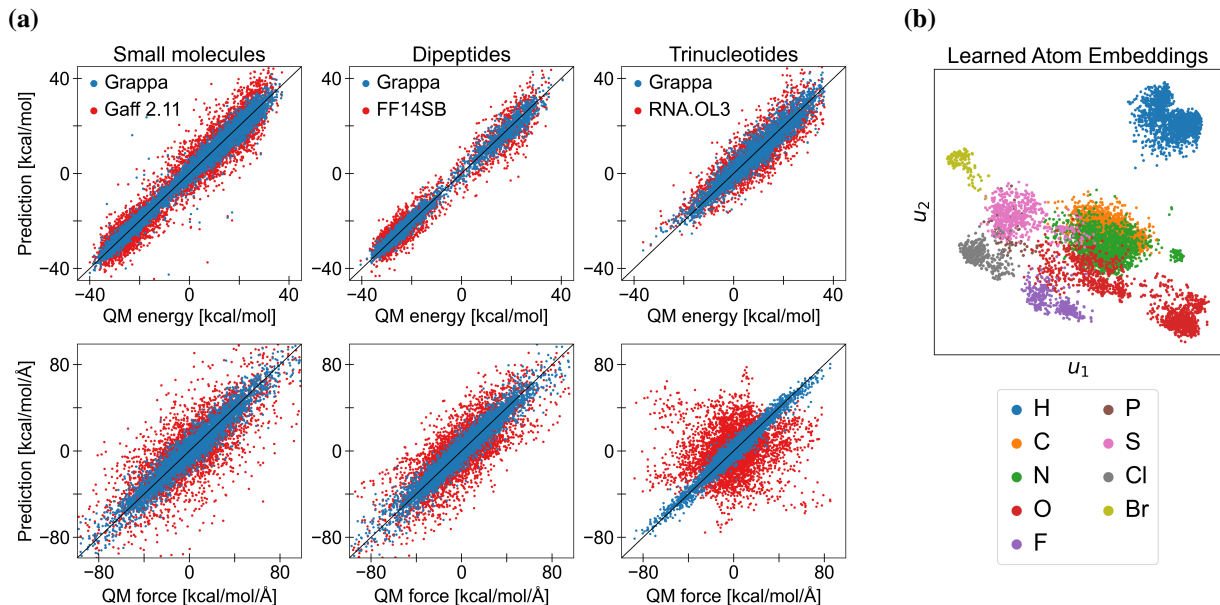


Figure 3: **(a)** Comparison of energy and force predictions of Grappa (model from Table 1) and established force fields for 10,000 randomly chosen conformations of test molecules from Espaloma’s SPICE-Pubchem, SPICE-Dipeptide and RNA-Trinucleotide dataset. **(b)** The two first principal components  $u_1$  and  $u_2$  of predicted atom embeddings from the Espaloma test dataset can be related to a combination of the main group and period in the periodic table of elements. Lines of constant main group or period are represented by approximate diagonals in latent space.

Dataset	Test Mols	Confs		Grappa AM1-BCC	Grappa ff99SB	Espaloma	ff14SB, RNA.OL3	Mean Predictor
SPICE-Dipeptide	67	2592	Energy	2.3	<b>2.2</b>	3.1	4.6	4.3
			Force	<b>5.5</b>	5.9	7.8	12.1	10.7
Radical-Dipeptide	28	275	Energy		<b>2.8</b>			7.4
			Force		<b>6.5</b>			23.6
HYP-DOP-Dipeptide	8	363	Energy		<b>2.3</b>			6.8
			Force		<b>5.6</b>			24.9
Uncapped-Dipeptide	12	600	Energy		<b>2.1</b>		3.7	6.5
			Force		<b>5.9</b>		11.7	25.3

Table 2: Accuracy of Grappa with nonbonded parameters from the AM1-BCC scheme, Grappa with nonbonded parameters from Amber ff99SB-ILDN, Espaloma 0.3 [10] and established MM force fields on a subset of test molecules from the Grappa-1.1 dataset. Both Grappa columns describe the same model that was trained to be consistent with both nonbonded parameter schemes on the whole Grappa-1.1 dataset; the performance on small molecules and RNA is similar to the one reported in Table 1 and can be found in the A5. As in Table 1, we report the RMSE of molwise-centered energies in kcal/mol and the componentwise RMSE of forces in kcal/mol/Å.

peptides, there is no baseline since, to the best of our knowledge, Grappa is the first MM force field that covers this part of chemical space.

#### 4. Force field validation

In this section, we demonstrate that Grappa is on par with established force fields when it comes to MD simulations of proteins over timescales of hundreds of nanoseconds and

that it captures the physics responsible for protein folding. All simulations mentioned in this section were performed with GROMACS, for which the Grappa package<sup>1</sup> provides a command line interface, briefly described in A.1. Using this interface (or a similar one for OpenMM), large biomolecular systems with over ten thousand atoms are parameterized within minutes on a CPU (Figure A6).

<sup>1</sup><https://github.com/hits-mbm-dev/grappa>

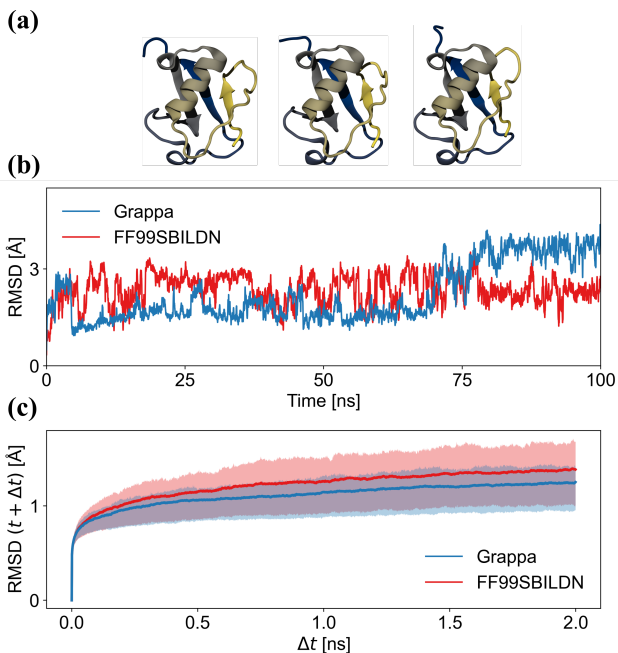


Figure 4: **(a)** Snapshots from an MD simulation of ubiquitin in water with Grappa after 25 ns, 50 ns and 75 ns with color-coded sequence position. **(b)** C-alpha root mean square deviation (RMSD) from the initial state during the simulation. **(c)** The mean C-alpha RMSD (and its 25th and 75th percentile) of 1000 pairs of frames that are separated by the time difference  $\Delta t$ .

#### 4.1. Grappa keeps large proteins stable during MD

A key quality check for a protein force field is if a native protein structure remains stable over time during an MD simulation. QM methods and E(3) equivariant neural networks suffer from the problem that while their end-to-end predictions are accurate, they often fail in yielding stable simulations because of diverging gradients of the potential energy surface when extrapolating beyond regions covered by the training dataset. Particularly over long timescales, the system might drift out of the range of validity of the model and small errors might accumulate, leading to instabilities of the system and a potential crash of the simulation. MM with its interpretable, physics-inspired energy function, with parameters which are conformation-independent, ensures a higher degree of stability, and we indeed did not observe simulation crashes.

However, obviously, it is not ensured a priori that macrostates such as protein folds remain stable during MD. We next assess Grappa’s capability of keeping protein folds close to their experimentally determined structure. As example system, we use ubiquitin (PDB ID: 1UBQ), which is a protein with 76 amino acids whose fold contains a beta-sheet and an alpha-helix. We perform a 100 nanoseconds

MD simulation of ubiquitin in aqueous solution with Grappa and Amber ff99SB-ILDN [17], for which details are given in A.6.2. We find that the C-alpha RMSD from the initial state is bounded by 4 Å in 100 ns simulation with both Grappa and Amber ff99SB-ILDN (Figure 4b), indicating that the folded state of the protein is stable. Structural fluctuations on timescales of up to 2 ns are smaller with Grappa (Figure 4c).

#### 4.2. Grappa can fold small proteins via MD

To assess Grappa’s coverage of conformational space, even far away from folded protein states, we investigate the folding trajectory of chignolin, a small protein with 10 amino acids. Starting from an unfolded state, we perform two 10 microseconds MD simulations of chignolin in aqueous solution with Grappa and with Amber ff99SB-ILDN [17] described in A.6.1. For the latter, it has already been shown that it can fold chignolin in a similar setup (Lindorff-Larsen et al. [25]), where the most populated cluster had a C-alpha RMSD of 1 Å to the experimentally determined reference structure (PDB ID: 5AWL).

We find that Grappa folds chignolin to the experimentally determined structure within the simulated microseconds, as can be seen in Figure 5. The most populated cluster has an RMSD of 0.8 Å to the reference structure while the most populated cluster of the Amber ff99SB-ILDN simulation has an RMSD of 0.9 Å, both of which are smaller than the resolution of the reference structure (1.1 Å). The folding trajectory of Grappa is qualitatively similar to the one of Amber ff99SB-ILDN, corroborating the validity of Grappa for protein simulations.

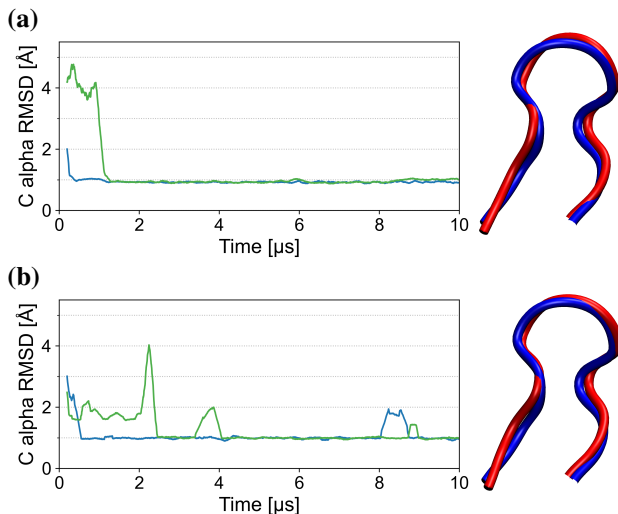


Figure 5: C alpha RMSD to the reference structure of chignolin during MD simulation with Grappa **(a)** and Amber ff99SB-ILDN **(b)** together with cluster centers (red) from the trajectory and the reference structure (blue).

## 5. Conclusions

With Grappa, we propose a machine learning framework to construct molecular mechanics force fields with state-of-the-art accuracy that can be used seamlessly in established MD engines. Our experiments show that Grappa is transferable to large biomolecules like proteins, which sets the stage for protein simulations at an unprecedented level of accuracy, with the same computational efficiency as established MM force fields but an error reduced by a factor of two.

Unlike most traditional MM force fields, Grappa is not specialized to a certain chemical species, but offers consistent parameterization of molecules from different regions of chemical space with a single model. We foresee Grappa as a general and versatile framework to extend the available parameter set at wish to new chemistries, being it to drugs, unusual lipids, complex sugars, or rare protein modifications.

While Grappa achieves high computational efficiency through molecular mechanics, it also inherits its fundamental limitations, including limited accuracy and the inability to directly model chemical reactions. However, Grappa is well suited for efficient reparametrization of large molecules that undergo local changes induced by chemical reactions, e.g. in kinetic Monte Carlo simulations [26]. This is due to both, Grappa’s finite field-of-view, which ensures locality on the molecular graph, as well as the lack of hand-crafted chemical features, which allows to apply the parametrization to cut-out regions of molecules.

While we consider the consistency with established non-bonded parameters an advantage of Grappa, an extension of our framework to nonbonded parameters is a straightforward next step. It would render Grappa fully independent from traditional MM force fields upon inference and could potentially improve its accuracy further.

## 6. Reproducibility statement

Grappa is released as open source software under the GNU General Public License v3.0 and is available at <https://github.com/hits-mbm-dev/grappa>. The repository contains the Grappa dataset along with the SMILES strings used for the train-val-test partition and configuration files to reproduce Table 1 and Table 2.

Folding and stability simulations can be reproduced using the repository at <https://github.com/LeifSeute/validate-grappa>, the creation of the dataset with uncapped peptides is documented at <https://github.com/LeifSeute/grappa-data-creation>.

Grappa utilizes PyTorch [27] and DGL [28] in its implementation.

## Author Contributions

**Leif Seute:** Methodology, Conceptualization, Software, Writing - Original Draft, Investigation, Visualization, Data Curation

**Eric Hartmann:** Conceptualization, Software, Verification, Visualization, Writing - Review and editing

**Jan Stühmer:** Formal analysis, Writing - Review and editing

**Frauke Gräter:** Supervision, Conceptualization, Writing - Review and editing

## Conflicts of interest

There are no conflicts to declare.

## Acknowledgements

This research was supported by the Klaus Tschira Foundation. The project has also received funding from the European Research Council (ERC) under the European Union’s Horizon 2020 research and innovation programme (grant agreement No. 101002812) [F.G.]. We thank Kai Riedmiller and Jannik Buhr for application and software related discussions, Fabian Grünewald and Camilo Aponte-Santamaria for discussions on future applications and Daniel Sucerquia for conversations on the role of internal coordinates in MM.

## References

- [1] Albert Musaelian, Simon Batzner, Anders Johansson, Lixin Sun, Cameron J. Owen, Mordechai Kornbluth, and Boris Kozinsky. Learning local equivariant representations for large-scale atomistic dynamics, 2022. URL <https://arxiv.org/abs/2204.05249>.
- [2] Ilyes Batatia, Dávid Péter Kovács, Gregor N. C. Simm, Christoph Ortner, and Gábor Csányi. Mace: Higher order equivariant message passing neural networks for fast and accurate force fields, 2023.
- [3] Guillem Simeon and Gianni de Fabritiis. TensorNet: Cartesian tensor representations for efficient learning of molecular potentials, 2023.
- [4] Oliver T. Unke, Martin Stöhr, Stefan Ganscha, Thomas Unterthiner, Hartmut Maennel, Sergii Kashubin, Daniel Ahlin, Michael Gastegger, Leonardo Medrano Sandonas, Alexandre Tkatchenko, and Klaus-Robert Müller. Accurate machine learned quantum-mechanical force fields for biomolecular simulations, 2022.
- [5] Kristof T. Schütt, Oliver T. Unke, and Michael

- Gastegger. Equivariant message passing for the prediction of tensorial properties and molecular spectra, 2021. URL <https://arxiv.org/abs/2102.03150>.
- [6] Yuanqing Wang, Josh Fass, Benjamin Kaminow, John E. Herr, Dominic Rufa, Ivy Zhang, Iván Pulido, Mike Henry, Hannah E. Bruce Macdonald, Kenichiro Takaba, and John D. Chodera. End-to-end differentiable construction of molecular mechanics force fields. *Chemical Science*, 13(41):12016–12033, 2022. doi: 10.1039/d2sc02739a. URL <https://doi.org/10.1039%2Fd2sc02739a>.
- [7] Ashish Vaswani, Noam Shazeer, Niki Parmar, Jakob Uszkoreit, Llion Jones, Aidan N. Gomez, Lukasz Kaiser, and Illia Polosukhin. Attention is all you need, 2023. URL <https://arxiv.org/abs/1706.03762>.
- [8] Mark James Abraham, Teemu Murtola, Roland Schulz, Szilárd Páll, Jeremy C. Smith, Berk Hess, and Erik Lindahl. Gromacs: High performance molecular simulations through multi-level parallelism from laptops to supercomputers. *SoftwareX*, 1-2:19–25, 2015. ISSN 2352-7110.
- [9] Peter Eastman, Mark S. Friedrichs, John D. Chodera, Randall J. Radmer, Christopher M. Bruns, Joy P. Ku, Kyle A. Beauchamp, Thomas J. Lane, Lee-Ping Wang, Diwakar Shukla, Tony Tye, Mike Houston, Timo Stich, Christoph Klein, Michael R. Shirts, and Vijay S. Pande. Openmm 4: A reusable, extensible, hardware independent library for high performance molecular simulation. *Journal of Chemical Theory and Computation*, 9(1):461–469, 2013. doi: 10.1021/ct300857j. URL <https://doi.org/10.1021/ct300857j>. PMID: 23316124.
- [10] Kenichiro Takaba, Iván Pulido, Mike Henry, Hugo MacDermott-Opeskin, John D. Chodera, and Yuanqing Wang. Espaloma-0.3.0: Machine-learned molecular mechanics force field for the simulation of protein-ligand systems and beyond, 2023.
- [11] Petar Veličković, Guillem Cucurull, Arantxa Casanova, Adriana Romero, Pietro Liò, and Yoshua Bengio. Graph attention networks, 2018. URL <https://arxiv.org/abs/1710.10903>.
- [12] Kaiming He, Xiangyu Zhang, Shaoqing Ren, and Jian Sun. Deep residual learning for image recognition, 2015.
- [13] Jimmy Lei Ba, Jamie Ryan Kiros, and Geoffrey E. Hinton. Layer normalization, 2016.
- [14] Shaked Brody, Uri Alon, and Eran Yahav. On the expressivity role of layernorm in transformers’ attention. *arXiv preprint arXiv:2305.02582*, 2023.
- [15] Seongjun Yun, Minbyul Jeong, Raehyun Kim, Jae-woo Kang, and Hyunwoo J. Kim. Graph transformer networks, 2020.
- [16] Araz Jakalian, David B. Jack, and Christopher I. Bayly. Fast, efficient generation of high-quality atomic charges. am1-bcc model: Ii. parameterization and validation. *Journal of Computational Chemistry*, 23(16):1623–1641, 2002. doi: <https://doi.org/10.1002/jcc.10128>. URL <https://onlinelibrary.wiley.com/doi/abs/10.1002/jcc.10128>.
- [17] K. Lindorff-Larsen, S. Piana, K. Palmo, P. Maragakis, J.L. Klepeis, R.O. Dror, and D.E. Shaw. Improved side-chain torsion potentials for the amber ff99sb protein force field. *Proteins*, 78(8):1950–1958, Jun 2010. doi: 10.1002/prot.22711. URL <https://doi.org/10.1002/prot.22711>.
- [18] Kristof T. Schütt, Pieter-Jan Kindermans, Huziel E. Saucedo, Stefan Chmiela, Alexandre Tkatchenko, and Klaus-Robert Müller. Schnet: A continuous-filter convolutional neural network for modeling quantum interactions, 2017. URL <https://arxiv.org/abs/1706.08566>.
- [19] Wojciech Marian Czarnecki, Simon Osindero, Max Jaderberg, Grzegorz Świrszcz, and Razvan Pascanu. Sobolev training for neural networks, 2017.
- [20] S. Boothroyd, P.K. Behara, O. Madin, D. Hahn, H. Jang, V. Gapsys, et al. Development and benchmarking of open force field 2.0.0 — the sage small molecule force field. *ChemRxiv*, 2022. doi: 10.1021/acs.jctc.3c00039. URL <https://doi.org/10.1021/acs.jctc.3c00039>. This content is a preprint and has not been peer-reviewed.
- [21] Xibing He, Viet Man, Wei Yang, Tai-Sung Lee, and Junmei Wang. A fast and high-quality charge model for the next generation general amber force field. *The Journal of chemical physics*, 153:114502, 09 2020. doi: 10.1063/5.0019056. URL <https://doi.org/10.1063/5.0019056>.
- [22] James A. Maier, Carmenza Martinez, Koushik Kasavajhala, Lauren Wickstrom, Kevin E. Hauser, and Carlos Simmerling. ff14sb: Improving the accuracy of protein side chain and backbone parameters from ff99sb. *Journal of Chemical Theory and Computation*, 11(8):3696–3713, 2015. ISSN 1549-9618. doi: 10.1021/acs.jctc.5b00255. URL <https://doi.org/10.1021/acs.jctc.5b00255>.

- [23] Marie Zgarbová, Michal Otyepka, Jiří Šponer, Arnošt Mládek, Pavel Banáš, Thomas E. Cheatham III, and Petr Jurečka. Refinement of the cornell et al. nucleic acids force field based on reference quantum chemical calculations of glycosidic torsion profiles. *Journal of Chemical Theory and Computation*, 7(9):2886–2902, 2011. ISSN 1549-9618. doi: 10.1021/ct200162x. URL <https://doi.org/10.1021/ct200162x>.
- [24] P. Eastman, P.K. Behara, D.L. Dotson, and et al. Spice, a dataset of drug-like molecules and peptides for training machine learning potentials. *Scientific Data*, 10(11), 2023. URL <https://doi.org/10.1038/s41597-022-01882-6>.
- [25] Kresten Lindorff-Larsen, Stefano Piana, Ron O. Dror, and David E. Shaw. How fast-folding proteins fold. *Science*, 334(6055):517–520, 2011. doi: 10.1126/science.1208351. URL <https://www.science.org/doi/abs/10.1126/science.1208351>.
- [26] Benedikt Rennekamp, Fabian Kutzki, Agnieszka Obarska-Kosinska, Christopher Zapp, and Frauke Gräter. Hybrid kinetic monte carlo/molecular dynamics simulations of bond scissions in proteins. *Journal of Chemical Theory and Computation*, 16(1):553–563, 2020. doi: 10.1021/acs.jctc.9b00786. URL <https://doi.org/10.1021/acs.jctc.9b00786>. PMID: 31738552.
- [27] Adam Paszke, Sam Gross, Francisco Massa, Adam Lerer, and et al. Pytorch: An imperative style, high-performance deep learning library, 2019.
- [28] Minjie Wang, Da Zheng, Zihao Ye, Quan Gan, Mufei Li, Xiang Song, Jinjing Zhou, Chao Ma, Lingfan Yu, Yu Gai, Tianjun Xiao, Tong He, George Karypis, Jinyang Li, and Zheng Zhang. Deep graph library: A graph-centric, highly-performant package for graph neural networks, 2020.
- [29] Djork-Arné Clevert, Thomas Unterthiner, and Sepp Hochreiter. Fast and accurate deep network learning by exponential linear units (elus), 2016.
- [30] Nitish Srivastava, Geoffrey Hinton, Alex Krizhevsky, Ilya Sutskever, and Ruslan Salakhutdinov. Dropout: A simple way to prevent neural networks from overfitting. *Journal of Machine Learning Research*, 15: 1929–1958, 06 2014.
- [31] Diederik P. Kingma and Jimmy Ba. Adam: A method for stochastic optimization, 2017.
- [32] Ilya Loshchilov and Frank Hutter. Sgdr: Stochastic gradient descent with warm restarts, 2017.
- [33] Arnaud Blondel and Martin Karplus. New formulation for derivatives of torsion angles and improper torsion angles in molecular mechanics: Elimination of singularities. *Journal of Computational Chemistry*, 17(9): 1132–1141, 1996.
- [34] D. G. A. Smith, L. A. Burns, and et al. Simmonett. Psi4 1.4: Open-source software for high-throughput quantum chemistry. *J. Chem. Phys.*, 2020. doi: 10.1063/5.0006002.
- [35] Berk Hess. P-LINCS: A parallel linear constraint solver for molecular simulation. 4(1):116–122. ISSN 1549-9618, 1549-9626. doi: 10.1021/ct700200b. URL <https://pubs.acs.org/doi/10.1021/ct700200b>.
- [36] Giovanni Bussi, Davide Donadio, and Michele Parrinello. Canonical sampling through velocity rescaling. 126(1):014101. ISSN 0021-9606, 1089-7690. doi: 10.1063/1.2408420.
- [37] M. Parrinello and A. Rahman. Polymorphic transitions in single crystals: A new molecular dynamics method. 52(12):7182–7190. ISSN 0021-8979. doi: 10.1063/1.328693. URL <https://doi.org/10.1063/1.328693>.
- [38] Shinya Honda, Toshihiko Akiba, Yusuke S. Kato, Yoshito Sawada, Masakazu Sekijima, Miyuki Ishimura, Ayako Ooishi, Hideki Watanabe, Takayuki Odahara, and Kazuaki Harata. Crystal structure of a ten-amino acid protein. *Journal of the American Chemical Society*, 130(46):15327–15331, 2008. doi: 10.1021/ja8030533. URL <https://doi.org/10.1021/ja8030533>. PMID: 18950166.

## A. Appendix

### A.1. The Grappa package

Grappa is released as open source software under the GNU General Public License v3.0 and is available at <https://github.com/hits-mbm-dev/grappa>.

It brings a command line interface to reparametrize a GRO-MACS topology file obtained from a traditional force field:

```
grappa_gmx -f topol.top -p new_topol.top
```

For OpenMM, we provide a class that can be used to reparametrize a system with Grappa:

```
from grappa import OpenmmGrappa

# use a traditional OpenMM forcefield
# to obtain a system from your topology
top, system = ...

# download a pretrained grappa model
ff = OpenmmGrappa.from_tag('grappa-1.1')

# re-parametrize the system using grappa
system = ff.parametrize_system(system, top)

# continue with usual workflow
```

Pretrained released models can be accessed by using a tag; the model weights are downloaded automatically from the respective release on GitHub. Released models also contain a dictionary with results on test datasets, a list of identifiers for molecules used for training and validation and a configuration file to reproduce training on the same dataset. For the reproduction of Table 1 and Table 2, one can use the tags ‘grappa-benchmark’ and ‘grappa-1.1.0’ respectively. Further details on the package can be found on GitHub.

### A.2. Model architecture

In this section, we provide a detailed description of the architecture of Grappa, including the graph attentional neural network and the symmetric transformer.

#### A.2.1. GRAPH ATTENTIONAL NEURAL NETWORK

Grappa’s graph attentional neural network (Figure A7) is a modification of the transformer architecture [7] for graphs, similar to the Graph Transformer Network [15], but e.g. omits the locality-breaking graph Laplacian eigenvectors as positional encoding. Instead, we encode the graph structure by constraining the attention mechanism to edges of the graph as in GAT [11], which enforces locality: In each attention update only neighboring nodes can influence each other. We use a multi-head dot-product attention mechanism and a 2-layer MLP as feed-forward network, where the hidden feature dimension is four times the node feature dimension.

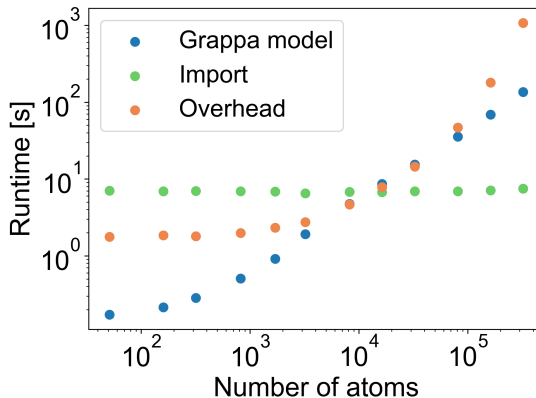


Figure A6: For molecules with up to 300,000 atoms, the runtime of a parameterization with the Grappa package in CPU mode is largely due to overhead. Due to its finite field-of-view, parametrizations can also be parallelised across several nodes by splitting the molecular graph into sub-graphs if necessary.

After initializing the node features  $\nu_i$  as described below, we apply a single nodewise linear layer followed by an exponential linear unit (ELU) [29],

$$\nu_i \leftarrow \text{ELU}(W\nu_i + b), \quad W \in \mathbb{R}^{d \times d_{\text{in}}}, \quad b \in \mathbb{R}^d, \quad (12)$$

Then, we apply  $L_{\text{GNN}}$  graph attentional layers, each of which is given by

$$\nu_i \leftarrow \text{LayerNorm}(\nu_i), \quad (13)$$

$$e_{ii'}^{(k)} = \left( W^{(k)} \nu_i \right) \cdot \left( W^{(k)} \nu_{i'} \right), \quad (14)$$

$$\text{att}_{ii'}^{(k)} = \frac{\exp\left(e_{ii'}^{(k)}\right)}{\sum_{n \in \mathcal{N}(i)} \exp\left(e_{in}^{(k)}\right)}, \quad (15)$$

$$V_i^{(k)} = \sum_{i' \in \mathcal{N}(i)} \text{att}_{ii'}^{(k)} W^{(k)} \nu_{i'}, \quad (16)$$

$$V_i \leftarrow \left( W_O \text{Concat} \left[ V_i^{(1)}, \dots, V_i^{(N_{\text{heads}})} \right] \right), \quad (17)$$

$$\nu_i \leftarrow \text{LayerNorm}(V_i) + \nu_i, \quad (18)$$

$$\nu_i \leftarrow \text{ELU}(W_2 \text{ELU}(W_1 \nu_i + b_1) + b_2) + \nu_i, \quad (19)$$

where  $\mathcal{N}(i)$  is the set of neighbors of node  $i$  including the node itself,  $(k)$  denotes the attention head and where the weights

$$W^{(k)} \in \mathbb{R}^{d \times d / N_{\text{heads}}}, \quad (20)$$

$$W_O \in \mathbb{R}^{d \times d}, \quad (21)$$

$$W_1 \in \mathbb{R}^{4d \times d}, \quad (22)$$

$$W_2 \in \mathbb{R}^{d \times 4d}. \quad (23)$$

and biases  $b_1, b_2$  are learnable and independent for each layer. We use dropout [30] on the node feature update in (18)

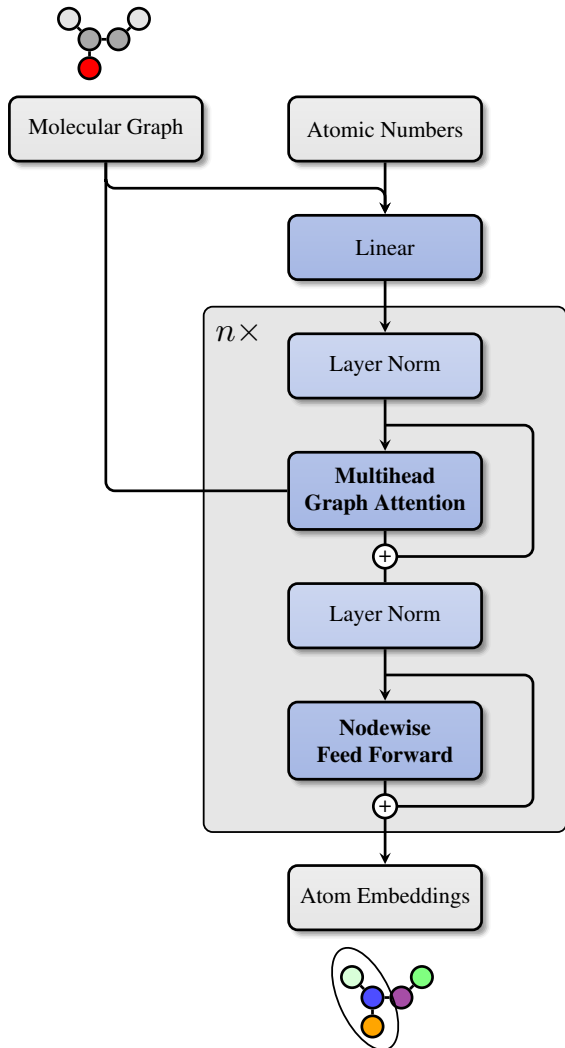


Figure A7: Grappa’s graph attentional neural network as described in Section A.2.1.

and (19). Finally, we project onto the output dimension  $d_{\text{emb}}$  by a linear layer,

$$\nu_i \leftarrow W\nu_i, W \in \mathbb{R}^{d_{\text{emb}} \times d}. \quad (24)$$

As initial node features we choose a one-hot encoding of the atomic number, a one-hot encoding of whether the node is in a loop, a one-hot encoding of the potential loop size and the degree of the node. Since Grappa only predicts bonded parameters, we have to ensure consistency with the nonbonded parameters from the traditional force field, which is why we one-hot encode the traditional force field used for the nonbonded contribution of the respective state if we train on a dataset that contains data from different nonbonded methods. We also include a sinusoidal encoding  $\tilde{Q}$  of the partial charges  $q$  as in the original transformer

architecture [7],

$$\tilde{Q}_{2i}(q) = \sin\left(\frac{q+2}{4} \cdot 10000 \frac{-2i}{32}\right), \quad (25)$$

$$\tilde{Q}_{2i+1}(q) = \cos\left(\frac{q+2}{4} \cdot 10000 \frac{-2i}{32}\right), \quad (26)$$

with  $i \in \{1, \dots, 16\}$ , which allows us to describe differently charged conformations of the same molecule without resorting to global or graph-symmetry breaking features like the formal charge.

#### A.2.2. SYMMETRIC TRANSFORMER

The graph attentional neural network is followed by four (parallel) symmetric transformers (Figure 2), one for each type of interaction, that is one for bond, one for angle, one for torsions and one for improper dihedral parameters. For each interaction (e.g. for each angle in the molecular graph), the node embeddings of the atoms involved is mapped to a set of respective MM parameters (e.g. equilibrium angle and force constant).

As described in Section 2.2, we add a symmetric positional encoding to the node features, as in (9), that is invariant under the desired set of permutations but can break symmetries that are not necessary to make the model more expressive while keeping equivariance under the permutations that we use for invariant pooling (10) later on. From the symmetries Eqs. 6-8, and from the considerations for improper dihedrals in Section A.4, we can derive the following positional encodings

$$\text{PE}_{\text{angle}} = (0, 1, 0), \quad (27)$$

$$\text{PE}_{\text{torsion}} = (0, 1, 1, 0), \quad (28)$$

$$\text{PE}_{\text{improper}} = (0, 1, 1, 0). \quad (29)$$

The bond positional encoding is not needed because the permutations of the bond parameters are the full group  $S_2$  and there is no symmetry that needs to be broken. For torsions and impropers, the positional encoding does not break all unnecessary symmetries, for example the symmetry  $ijkl \rightarrow ljk i$  is still present with positional encoding, and will be broken later.

We then apply a transformer acting one nodes that represent the atoms involved in the interaction, that is, after a projection on features of dimension  $d_T$ ,

$$\nu_i \leftarrow \text{ELU}(W\nu_i + b), W \in \mathbb{R}^{d_T \times d_{\text{emb}}}, b \in \mathbb{R}^{d_T}, \quad (30)$$

we apply  $L_T$  transformer layers, each of which is given by scaled dot-product attention with  $N_{\text{T-heads}}$  heads and a 2-layer MLP with hidden dimension  $4d_T$ , skip connections, dropout and layer normalization as in the original transformer architecture [7].

We then apply a symmetry pooling operation by passing permuted versions of concatenated node embeddings to a  $L_{\text{pool}}$ -layer MLP with hidden dimension  $d_{\text{pool}}$  and summing over all permutations  $\sigma$  in the respective symmetry group  $\mathcal{P}$ ,

$$z_{ij\dots} = \sum_{\sigma \in \mathcal{P}} \text{MLP}([\nu_{\sigma(i)}, \nu_{\sigma(j)}, \dots]), \quad (31)$$

The two dimensional scores  $z_{ij}$  for bonds and  $z_{ijk}$  for angles are finally mapped to the range of the respective set of MM parameters by scaled and shifted versions of ELU and the sigmoid function,

$$k_{ij} = \text{ToPos}(z_{ij, 0}), \quad (32)$$

$$r_{ij}^{(0)} = \text{ToPos}(z_{ij, 1}), \quad (33)$$

$$k_{ijk} = \text{ToPos}(z_{ijk, 0}), \quad (34)$$

$$\theta_{ijk}^{(0)} = \text{ToRange}_{(0, \pi)}(z_{ijk, 0}), \quad (35)$$

where  $\text{ToPos}$  and  $\text{ToRange}_{(0, \pi)}$  are defined in Section A.2.3 and  $z_{\dots, n}$  denotes the  $n$ -th entry of the score vector  $z_{\dots}$ . For dihedral force constants, the  $2n_{\text{periodicity}}$  dimensional scores  $z_{ijkl}$  are fed through a sigmoid gate to make the model more expressive for small force constants,

$$k_{ijkl, m} = z_{ijkl, 2m+1} \times \text{sigmoid}(z_{ijkl, 2m}). \quad (36)$$

### A.2.3. SCALING OF NEURAL NETWORK OUTPUTS

To map the scores predicted from our model to the range of the respective MM parameter, we use scaled and shifted versions of the sigmoid function for mapping to a specified interval and of ELU for mapping to positive values. We choose these functions because they are differentiable and, in contrast to the exponential, only grow linearly for large inputs, which can help to stabilize training. To allow the model to predict scores that are of order unity, or approximately normally distributed, we choose the scaling and shifting parameters in such a way that a normally distributed input would lead to an output distribution whose mean and standard deviation are close to a given target mean  $\mu$  and standard deviation  $\sigma$ . We choose this target standard deviation by calculating mean and standard deviation of traditional MM force field parameters on a given subset of the training data, except for equilibrium angles, where we restrict  $\mu$  to  $\pi/2$ .

For mapping to positive values, we use

$$\text{ToPos}[\mu, \sigma](z) = \sigma \left( \text{ELU} \left( \frac{\mu}{\sigma} + z - 1 \right) + 1 \right), \quad (37)$$

and for mapping to a specified interval  $(0, \gamma)$ , we restrict ourselves to the case  $\mu = \gamma/2$  use

$$\text{ToRange}[\gamma/2, \sigma]_{(0, \gamma)}(z) = \gamma \text{sigmoid} \left( \frac{4\sigma}{\gamma} z \right). \quad (38)$$

We can see that the mean and standard deviation of the output are indeed close to the target mean and standard deviation if we consider the asymptotic behavior of the sigmoid function and ELU as their input approaches zero,

$$\text{ELU}(x) \sim x + \mathcal{O}(x^2) \quad \text{as } x \rightarrow 0, \quad (39)$$

$$\text{sigmoid}(x) \sim \frac{1}{2} + \frac{x}{4} + \mathcal{O}(x^2) \quad \text{as } x \rightarrow 0, \quad (40)$$

which follows from the Taylor expansion of the ELU and sigmoid functions around zero. Thus, using that  $z$  has vanishing mean and unit standard deviation, we have indeed, to first order in  $z$ ,

$$\langle \text{ToRange}(z) \rangle \approx \gamma(1/2 + 4\sigma/\gamma \langle z \rangle) = \gamma/2$$

and

$$\begin{aligned} \text{Var}[\text{ToRange}(z)] &\approx \langle \gamma^2 \left( 1/2 + \frac{\sigma}{\gamma} z \right)^2 \rangle - \gamma^2/4 \\ &= \gamma^2 \left( 1/4 + \frac{\sigma}{\gamma} \langle z \rangle + \sigma^2/\gamma^2 \langle z^2 \rangle - 1/4 \right) = \sigma^2. \end{aligned}$$

For mapping to positive values, we expand ELU in  $\mu/\sigma - 1 + z$  around zero, which is reasonable if  $\mu/\sigma \approx 1$ , and find in analogy that target mean and standard deviation are recovered to first order in  $\mu/\sigma - 1 + z$ .

### A.3. Hyperparameters and training details

For all models discussed in this work, we use the hyperparameters listed in Table A3 and a dihedral periodicity of  $n_{\text{periodicity}} = 3$ . All relative weights between energies, forces and MM parameters rely on units formed by kcal/mol, Å and radian. We train the models using the Adam [31] optimizer with  $\epsilon = 10^{-8}$ ,  $\beta_1 = 0.9$ ,  $\beta_2 = 0.999$ .

First, we train for 2 epochs on traditional MM parameters only, which can be interpreted as a form of pretraining that is efficient in bringing the model in a state where the gradients of the QM-part of the loss functions are informative. We start the training on energies and forces with  $\lambda_{\text{trad}} = 10^{-3}$ , which we set to zero after 100 epochs, preventing the model from converging towards unphysical local minima of the QM-part of the loss function. When changing weights of terms of the loss function as described above, we re-initialize the optimizer with random moments and apply a warm restart [32], during which we linearly increase the learning rate in 500 training steps to decorrelate the optimizer state from the gradient updates of the previous loss function. Besides pretraining on traditional MM parameters directly, we have found penalizing large torsion and improper force constants  $\xi^{(\text{dih})}$  to benefit generalizability across conformational space.

As validation loss, we use a linear combination of the energy and force root mean squared error (RMSE) on the sub-datasets (the rows in Table 1), averaged over all sub-datasets,

Hyperparameter	Variable	Value
Graph Neural Network		
Layers	$L_{\text{GNN}}$	7
Hidden dimension	$d$	512
Attention heads	$N_{\text{heads}}$	16
Embedding dimension	$d_{\text{emb}}$	256
Dropout probability		0.3
Symmetric Transformer		
Transformer layers	$L_T$	3
Transformer hidden dim	$d_T$	512
Attention heads	$N_{T\text{-heads}}$	8
Pooling layers	$L_{\text{pool}}$	3
Pooling hidden dim	$d_{\text{pool}}$	256
Dropout probability		0.5
Training setup		
Learning rate		$1.5 \times 10^{-5}$
Molecules per batch		32
States per molecule		32
Force weight	$\lambda_F$	0.8
Dihedral $L_2$ weight	$\lambda_{\text{dih}}$	$10^{-3}$
Traditional MM weight	$\lambda_{\text{trad}}$	0

Table A3: The hyperparameters used for training the Grappa models in this work.

with a weight of 1 for the energy RMSE and 3 for the force RMSE to prevent overfitting on a molecule type. We use this validation loss for early stopping and for learning rate scheduling. For the model trained on the Espaloma dataset (Table 1), the validation loss did not improve after 1000 epochs, which corresponds to one day of training on a single NVIDIA RTX 6000 Ada GPU.

#### A.4. Improper dihedrals

As discussed in Section 2.2, we postulate that the energy contributions from the different interactions are symmetric under certain permutations of the embeddings and spatial positions of the atoms involved. These permutations are given by the isomorphisms of the respective subgraph that describes the interaction. In the case of angles, bonds and torsions, these symmetries are given by Eqs. 6-8, for improper dihedrals, the symmetries are given by all six permutations that leave the central atom invariant, as can be seen from the structure of the subgraphs in Figure A8. For bonds, angles and torsions, the interaction coordinates distance, angle and the cosine of the dihedral angle are invariant under the respective permutations, which is why we can construct an invariant energy contribution simply by enforc-

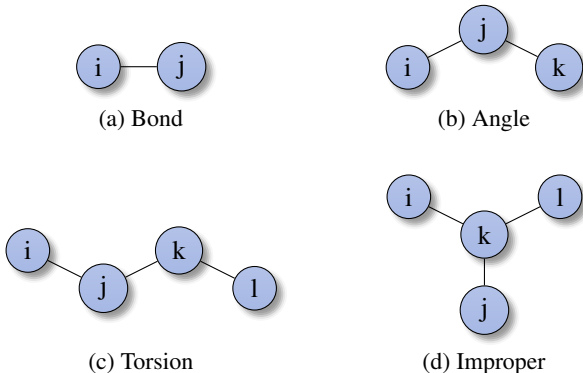


Figure A8: The subgraphs of the molecular graph that correspond to bonded MM interactions

ing invariance of the MM parameters under the respective permutations.

For improper dihedrals, this is not the case, as the dihedral angle is not invariant under all six permutations mentioned above and a model with improper force constants that are invariant under these permutations would not have invariant improper energy contributions. In Grappa, we solve this problem by introducing more terms for improper dihedrals. For example

$$E_{\text{improper}} = k_{ijkl} \cos(\phi_{ijkl}) + k_{jikl} \cos(\phi_{jikl}), \quad (41)$$

is invariant under the permutation  $ijkl \rightarrow jikl$ , which can be generalized to all six improper permutations. It turns out that we can reduce the number of additional terms to two by using another symmetry of the dihedral angle,

$$\cos(\phi_{ijkl}) = \cos(\phi_{ljki}), \quad (42)$$

which can be seen from the formula for the dihedral angle in [33]. This symmetry allows us to identify pairs of terms that are transformed into each other under the permutation  $ijkl \rightarrow ljki$  and use a force constant that is invariant under this permutation,

$$k_{ijkl}^{(\text{improper})} = k_{ljki}^{(\text{improper})}. \quad (43)$$

#### A.5. Datasets

##### A.5.1. ESPALOMA DATASET

We reproduce the dataset used to train and evaluate Espaloma 0.3 [10] by downloading the published, preprocessed data<sup>2</sup>. The preprocessing entails filtering out high-energy conformations as detailed in [10]. As in Espaloma, our train-val-test partitioning procedure relies on the unique

<sup>2</sup>[https://github.com/hits-mbm-dev/grappa/blob/master/dataset\\_creation/get\\_espaloma\\_split/load\\_esp\\_ds.py](https://github.com/hits-mbm-dev/grappa/blob/master/dataset_creation/get_espaloma_split/load_esp_ds.py)

isomeric SMILES strings of the molecules, which are included in the dataset. We reproduce<sup>3</sup> the partitioning from Espaloma 0.3<sup>4</sup> with the same random seed.

For the calculation of the RMSE in Table 1 and Table 2, we subtract the mean predicted energy for each molecule and for each force field since we are only interested in relative energy differences (and the mean is the unique global shift that minimizes the RMSE). For forces, we report the componentwise RMSE

$$\text{RMSE} \equiv \sqrt{\frac{1}{3N} \sum_{i=1}^N \sum_{j=1}^3 (f_{ij} - f_{ij}^{(\text{ref})})^2}$$

as it is done in Espaloma 0.3.

#### A.5.2. DATASET CREATION

Scripts for the creation of the datasets can be found at <https://github.com/LeifSeute/grappa-data-creation>. We use the Amber ff99SB-ILDN [17] force field for sampling the states and Psi4 [34] for the single point QM calculations. For sampling radical peptide states, we use a preliminary Grappa model trained on optimization trajectories and torsion scans of radical peptides. The radical peptides are what we call hydrogen-atom-transfer (HAT) type radicals, that is, they are formed by removing a single hydrogen from a peptide. For the nonbonded contribution, we use the same Lennard-Jones parameters as for the original peptide and add the partial charge of the hydrogen in the original peptide to the heavy atom it was attached to.

### A.6. MD simulations

All folding and stability simulations are performed with GROMACS version 2023 [8] using the Amber ff99SB-ILDN force field [17] or Grappa-1.1 with Amber ff99SB-ILDN nonbonded parameters and the TIP3P water model. 2 fs time steps with LINCS constraints [35] on H-bonds were employed. Simulations were run at 300K and 1 bar, maintained by the v-rescale thermostat [36] and Parrinello-Rahman pressure coupling [37]. We apply a Coulomb and Lennard-Jones cutoff of 1.0nm. After system preparation, energy minimization, NVT and NPT equilibration simulations are conducted. The code for reproducing the simulations can be found at <https://github.com/LeifSeute/validate-grappa>.

<sup>3</sup>[https://github.com/hits-mbm-dev/grappa/blob/master/dataset\\_creation/get\\_espaloma\\_split/load\\_esp\\_ds.py](https://github.com/hits-mbm-dev/grappa/blob/master/dataset_creation/get_espaloma_split/load_esp_ds.py)

<sup>4</sup><https://github.com/choderalab/refit-espaloma/blob/main/openff-default/02-train/joint-improper-charge/charge-weight-1.0/train.py>, commit 3ccc44d

#### A.6.1. FOLDING SIMULATIONS

For the folding simulations, we follow the simulation system setup of Lindorff-Larsen *et al.* [25] From a completely extended solvated structure, we minimize and equilibrate, followed by a short MD simulation, in which the end-to-end distance of the protein usually reduces. We pick a state with low end-to-end distance and use it as starting point for the actual folding simulation in which we can choose the simulation box smaller, reducing the computational cost. For the folding simulations of a mutant of chignolin [38] (PDB ID: 5AWL) with the sequence YYDPETGTWY, we choose a box size of 40 Å, and neutralize the system with two sodium ions.

#### A.6.2. STABILITY SIMULATIONS

The simulations of ubiquitin (PDB ID: 1UBQ) are evaluated by calculating a moving average over 0.05 ns of the C-alpha RMSD to the initial structure (Figure 4b). We also calculate the statistics of the C-alpha RMSD as function of time difference between two states. To this end, we sample 1,000 states from the trajectory for each time difference and calculate the mean C-alpha RMSD between the states.

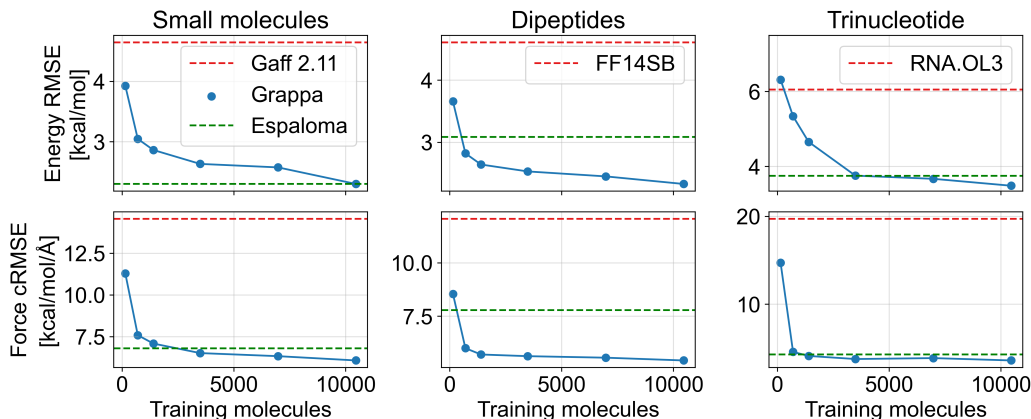


Figure A9: Test RMSE of Grappa (blue), trained on a fraction of the Espaloma train dataset, compared with the RMSE of Espaloma (green) trained on the full dataset and the RMSE of established force fields.

Dataset	Test Mols	Confs		Grappa	Espaloma	Gaff-2.11	ff14SB, RNA.OL3	Mean Predictor
BOLTZMANN SAMPLED								
SPICE-Pubchem	1411	60853	<i>Energy</i>	<b>2.3</b> ± 0.1	<b>2.3</b> ± 0.1	4.6		18.4
			<i>Force</i>	<b>6.1</b> ± 0.3	6.8 ± 0.1	14.6		23.4
SPICE-DES-Monomers	39	2032	<i>Energy</i>	<b>1.3</b> ± 0.1	1.4 ± 0.3	2.5		8.2
			<i>Force</i>	<b>5.2</b> ± 0.2	5.9 ± 0.5	11.1		21.3
SPICE-Dipeptide	67	2592	<i>Energy</i>	<b>2.3</b> ± 0.1	3.1 ± 0.1	4.5	4.6	18.7
			<i>Force</i>	<b>5.4</b> ± 0.1	7.8 ± 0.2	12.9	12.1	21.6
RNA-Diverse	6	357	<i>Energy</i>	<b>3.3</b> ± 0.2	4.2 ± 0.3	6.5	6.0	5.4
			<i>Force</i>	<b>3.7</b> ± 0.04	4.4 ± 0.1	16.7	19.4	17.1
RNA-Trinucleotide	64	35811	<i>Energy</i>	<b>3.5</b> ± 0.1	3.8 ± 0.2	5.9	6.1	5.3
			<i>Force</i>	<b>3.6</b> ± 0.01	4.3 ± 0.1	17.1	19.7	17.7
TORSION SCAN								
Gen2-Torsion	131	21890	<i>Energy</i>	1.7 ± 0.2	<b>1.6</b> ± 0.3	2.7		4.7
			<i>Force</i>	<b>4.0</b> ± 0.4	4.7 ± 0.6	9.4		5.5
Protein-Torsion	9	6624	<i>Energy</i>	2.2 ± 0.4	<b>1.9</b> ± 0.2	3.0		3.5
			<i>Force</i>	3.8 ± 0.5	<b>3.5</b> ± 0.3	9.7		5.1
OPTIMIZATION								
Gen2-Opt	154	40055	<i>Energy</i>	1.8 ± 0.2	<b>1.7</b> ± 0.5	3.0		3.9
			<i>Force</i>	<b>3.8</b> ± 0.2	4.5 ± 0.8	9.7		5.1
Pepconf-Opt	55	14884	<i>Energy</i>	3.2 ± 0.3	<b>2.8</b> ± 0.3	5.1	4.1	6.3
			<i>Force</i>	<b>3.6</b> ± 0.2	4.0 ± 0.4	10.2	10.2	5.3

Table A4: Accuracy of Grappa, Espaloma 0.3 [10] and established MM force fields on test molecules from the Espaloma dataset. We report the RMSE of molwise-centered energies in kcal/mol and the componentwise RMSE of forces in kcal/mol/Å. Gaff-2.11 [21] is a general-purpose force field, ff14SB [22] is an established protein force field and RNA.OL3 [23] is specialized to RNA. As in Espaloma, we bootstrap the set of test molecules 1000 times and report mean and standard deviation of the RMSEs.

Grappa - A Machine Learned Molecular Mechanics Force Field

Dataset	Test Mols	Confs		Grappa AM1-BCC	Grappa ff99SB	Espaloma	ff14SB, RNA.OL3	Mean Predictor
BOLTZMANN SAMPLED								
SPICE-Pubchem	1411	60853	<i>Energy</i>	<b>2.3</b>		<b>2.3</b>		18.6
			<i>Force</i>	<b>6.1</b>		6.8		23.5
SPICE-DES-Monomers	39	2032	<i>Energy</i>	<b>1.3</b>		1.4		8.3
			<i>Force</i>	<b>5.3</b>		5.9		21.3
SPICE-Dipeptide	67	2592	<i>Energy</i>	2.3	<b>2.2</b>	3.1	4.6	4.3
			<i>Force</i>	<b>5.5</b>	5.9	7.8	12.1	10.7
RNA-Diverse	6	357	<i>Energy</i>	<b>3.4</b>		4.2	6.0	5.8
			<i>Force</i>	<b>3.7</b>		4.4	19.4	17.0
RNA-Trinucleotide	64	35811	<i>Energy</i>	<b>3.6</b>		3.8	6.1	5.8
			<i>Force</i>	<b>3.6</b>		4.3	19.7	17.8
Radical-Dipeptide	28	275	<i>Energy</i>		<b>2.8</b>			7.4
			<i>Force</i>		<b>6.5</b>			23.6
HYP-DOP-Dipeptide	8	363	<i>Energy</i>		<b>2.3</b>			6.8
			<i>Force</i>		<b>5.6</b>			24.9
Uncapped-Dipeptide	12	600	<i>Energy</i>		<b>2.1</b>		3.7	6.5
			<i>Force</i>		<b>5.9</b>		11.7	25.3
TORSION SCAN								
Gen2-Torsion	131	21890	<i>Energy</i>	1.8		<b>1.6</b>		4.8
			<i>Force</i>	<b>4.0</b>		4.7		5.5
Protein-Torsion	9	6624	<i>Energy</i>	2.2	2.2	<b>1.9</b>		2.4
			<i>Force</i>	3.9	5.2	<b>3.5</b>		9.6
OPTIMIZATION								
Gen2-Opt	154	40055	<i>Energy</i>	1.8		<b>1.7</b>		3.9
			<i>Force</i>	<b>3.8</b>		4.5		5.1
Pepconf-Opt	55	14884	<i>Energy</i>	3.2	<b>2.7</b>	2.8	4.1	3.5
			<i>Force</i>	<b>3.7</b>	4.5	4.0	10.2	9.6

Table A5: Accuracy of Grappa with nonbonded parameters from the AM1-BCC scheme, Grappa with nonbonded parameters from Amber ff99SB-ILDN, Espaloma 0.3 [10] and established MM force fields on test molecules of the Grappa-1.1 dataset. We report the RMSE of molwise-centered energies in kcal/mol and the componentwise RMSE of forces in kcal/mol/Å.